

Site-Selective Optical Coupling of PbSe Nanocrystals to Si-Based Photonic Crystal Microcavities

Andras G. Pattantyus-Abraham,^{†,§,#} Haijun Qiao,^{†,#} Jingning Shan,^{‡,||}
Keith A. Abel,[‡] Tian-Si Wang,[†] Frank C. J. M. van Veggel,[‡] and Jeff F. Young^{*,†}

Department of Physics and Astronomy, University of British Columbia,
Vancouver, British Columbia, V6T 1Z1 Canada, and Department of Chemistry,
University of Victoria, Victoria, British Columbia, V8W 3 V6, Canada

Received March 26, 2009; Revised Manuscript Received June 23, 2009

ABSTRACT

A novel method for patterning optically active colloidal PbSe nanocrystals on Si surfaces is reported. Oleate-capped PbSe nanocrystals were found to adhere preferentially to H-terminated Si surfaces over oxide and alkyl-terminated Si surfaces. Scanning probe lithography was used to oxidize locally a dodecyl monolayer on the Si surface of a silicon-on-insulator wafer prepatterned with photonic crystal microcavities. Aqueous HF was then used to remove the oxide and expose H-terminated Si areas, yielding patterned PbSe nanocrystals on the Si surface after exposure to a nanocrystal solution. This patterning technique allows for the selective deposition of PbSe nanocrystals at the main antinode of the silicon-based microcavities. More than a 10-fold photoluminescence enhancement due to the cavity-nanocrystal coupling was observed.

The integration of nanoscale functional elements, such as organic molecules, biomolecules, and nanoparticles, into micrometer- and submicrometer-scale devices is one of the challenges of present day science and engineering.^{1–3} We describe here a method for patterned deposition of 5 nm PbSe nanocrystals with pattern feature sizes below 100 nm on Si surfaces. In particular, we demonstrate integration with Si-based photonic crystal microcavities for the purpose of forthcoming cavity quantum electrodynamics (CQED) experiments^{4–6} in which an electronic two-level system is coupled to a silicon photonic cavity. Such systems present a route toward the realization of devices for quantum information processing.⁷

Free-standing Si-based photonic crystal microcavities (Figure 1A) are readily prepared from silicon-on-insulator (SOI) substrates, and Q values in excess of 10^6 have recently been reported for such microcavities.⁸ These microcavities are usually designed to work in the near-infrared between 1500 and 1600 nm to take advantage of tunable lasers and detectors operating in this range and also to avoid the water absorption band (1350–1450 nm). The SOI substrates are

less expensive and toxic than the corresponding III–V substrates and allow for eventual integration with standard Si-based microelectronics. However, for CQED experiments, the high quality self-assembled quantum dots prepared by epitaxial growth on III–V substrates (e.g., InGaAs on InP, InGaAs on AlGaAs) are not available in Si, although Ge quantum dots are in development.⁹

Commercial infrared-emission applications rely on devices fabricated epitaxially from direct band gap semiconductors, which cannot be grown with high quality on Si. An alternative that does allow direct integration with Si is the use of solution-grown infrared emitters such as colloidal semiconductor nanocrystals, which are prepared using simple wet chemistry.^{10,11} These nanocrystals have fundamental excitonic transitions at energies higher than their bulk host material's bandgap due to the quantum confinement effect. A number of compound semiconductors have small bulk bandgaps that can be shifted into the near-infrared,^{12–14} for example, PbS, PbSe, and PbTe. Their suitability for cavity QED experiments and quantum information processing has recently been discussed,⁷ and in particular the homogeneous line width of the excitonic transition as well as spectral diffusion remain issues to be addressed.

Colloidal semiconductor nanocrystals have been coupled in a nonselective manner to GaAs- and Si-based photonic crystal microcavities.^{15–20} However, the ideal realization would involve coupling a single nanocrystal to the microcavity near the maximum of the electric field intensity of

* To whom correspondence should be addressed. E-mail: young@phas.ubc.ca.

[†] University of British Columbia.

[‡] University of Victoria.

[§] Current address: Department of Electrical and Computer Engineering, University of Toronto, Toronto, ON, Canada, M5S 3G4.

[#] Current address: Department of Mechanical and Aerospace Engineering, Princeton University, Princeton, New Jersey 08544.

^{||} These authors contributed equally to this work.

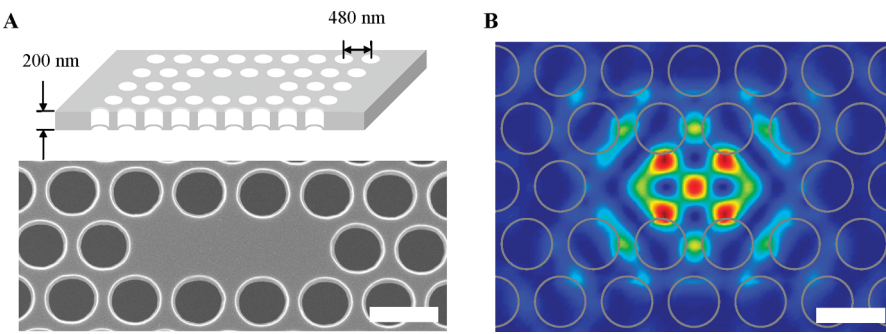


Figure 1. (A) Illustration and scanning electron micrograph of Si-based photonic crystal microcavity. (B) Calculated total electric field intensity at the microcavity surface with the outline of the etched holes overlaid. The scale bars are 500 nm long.

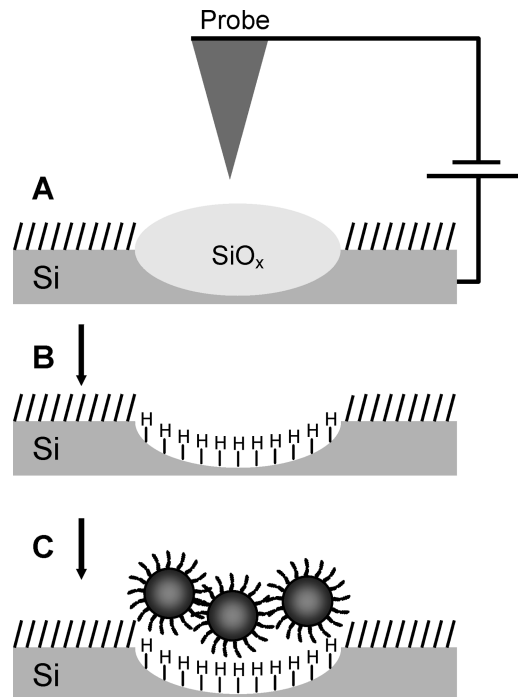
the photonic mode. For the three-missing-hole microcavity design considered here,²¹ the calculated electric field intensity at the surface is presented in Figure 1B. Local maxima are present at the center and near the four closest etched holes. The coupling between the trapped photon and a nanocrystal would be maximized within a radius of ~ 50 nm of any of these maxima. In this work, we present a novel method for patterning PbSe nanocrystals on the Si surface via scanning probe lithography on length scales below 100 nm. We apply this technique to control the coupling of PbSe semiconductor nanocrystals to the cavity modal field on Si-based photonic crystal microcavities. The luminescence of such cavity-coupled nanocrystals is also reported, and we quantify the enhancement afforded by the patterning process.

We adopted a coupling strategy exploiting the affinity of H-terminated Si surface for oleate-capped PbSe nanocrystals. This approach allows nanocrystal adhesion to the surface nominally without any changes to the nanocrystal surface, such as the introduction of a new ligand. Site-selective nanocrystal grafting further requires the creation of a chemically patterned surface. Nanocrystals have been patterned on the submicrometer and micrometer scale using e-beam lithography²² and photolithography.²³ In our approach, scanning probe lithography^{24–27} allows both nondestructive, high resolution imaging and modification of the substrate. Accurate registry with pre-existing surface patterns was obtained by mitigating the nonlinear behavior of the piezoelectric scanner using a proper feedback scheme.²⁸

Selective Adhesion of Colloidal PbSe Nanocrystals to Si Substrates. Our patterning process is depicted in Scheme 1. We used scanning probe lithography and the selective adhesion of oleate-capped PbSe nanocrystals to H-Si(100) areas to achieve site-specific grafting. The oleate ligands incorporate an alkene moiety that is in principle amenable to the hydrosilylation reaction²⁹ with H-Si. In investigating this avenue for grafting, we have found that oleate-capped PbSe nanocrystals adhere quite well to H-Si(100) ($\sim 3 \times 10^3$ nanocrystals/ μm^2) but poorly to oxidized or dodecyl-terminated Si (~ 10 nanocrystals/ μm^2) (Figure 2). This selectivity was achieved by simply covering the H-Si substrate with nanocrystal solution and then washing away excess nanocrystals with solvent. This avoided mechanical cleaning (wiping,^{30,31} ultrasonication) that could damage sensitive surface structures.

Scheme 1. Nanocrystal Patterning Process (Not to Scale):

- (A) Local Oxidation of Dodecyl Monolayer and Si Surface,
- (B) Oxide Removal by Aqueous HF Treatment,
- (C) Nanocrystal Adhesion to H-Terminated Areas



The lack of adhesion to alkyl-Si and oxidized Si does suggest a specific chemical interaction with the H-Si surface. However, no evidence of Si-C bonds was found by X-ray photoelectron spectroscopy (XPS), and the adhesion process appears to be complete within seconds. These observations

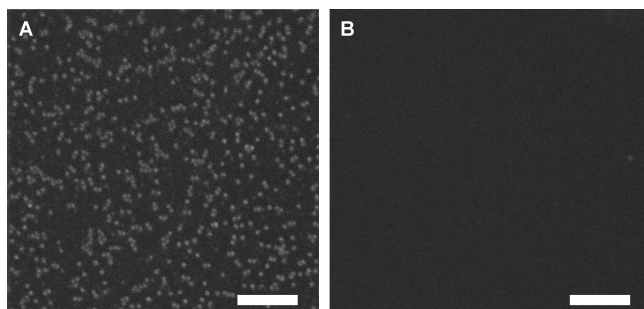


Figure 2. Scanning electron micrographs depicting PbSe nanocrystal adhesion to different surfaces. (A) H-Si, (B) dodecyl-Si. Scale bars are 100 nm long.

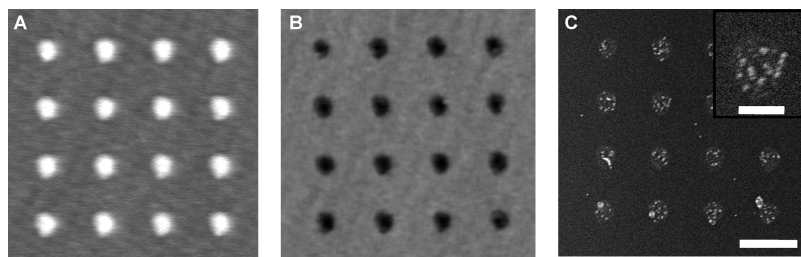


Figure 3. Site-selective grafting process of PbSe nanocrystals. Atomic force micrographs of (A) 2.5 nm high oxide dots on dodecyl-SOI, (B) 1.5 nm deep etched pits after 2% aqueous HF treatment, both are $1 \times 1 \mu\text{m}^2$, and (C) scanning electron micrograph of patterned PbSe nanocrystals. The scale bar is 200 nm long. The inset shows a magnified view of one of the patterned spots with a scale bar of 50 nm.

are in contrast with the report for Au nanocrystals grafted to Si, where the Si–C bond was detected by XPS, and the reaction progressed with time and heating.³² The surface hydrosilylation reaction is normally thought to be initiated through thermal or photochemical activation of the surface Si–H bond.²⁹ Thus it is possible that the initial adhesion of PbSe nanocrystals to Si is mediated instead by van der Waals forces between the nanocrystal and the H–Si surface. For the adhesion process to proceed, the interaction between the nanocrystal and the surface must be larger than the interaction between the nanocrystal and the solvent. In the presence of either an alkyl monolayer or native oxide, the van der Waals interactions with the solvent would dominate the weaker interaction with the substrate surface.

The behavior of PbSe nanocrystals on the dodecyl- and H–Si surfaces stands in contrast with the recent work of Graaf et al., who reported the patterning of trioctyl phosphine oxide (TOPO)-capped CdSe/ZnS nanocrystals using dodecyl-derivatized Si substrates.²⁵ The CdSe/ZnS nanocrystals were reported to attach in higher density to the dodecyl-coated regions, and in effect the dodecyl moiety acted as a negative resist for CdSe/ZnS patterning. In our work, the same surface molecule acted as a positive resist for PbSe patterning, where the modified areas attract nanocrystals. As both the oleate- and the TOPO-capped nanocrystals present a hydrophobic surface, this again suggests that the surface binding process is mediated by other than straightforward hydrophobic/hydrophilic interactions. Surface dipoles on PbSe nanocrystals have been proposed as a driving force for self-assembly³³ and could also play a role in the process reported here.

Patterned Deposition of Colloidal PbSe Nanocrystals. The selective adhesion of oleate-capped PbSe nanocrystals to H–Si was exploited to obtain patterned deposition. The preparation of H–Si patterns on Si may be accomplished using most standard lithographic techniques with thick resists, but scanning probe lithography requires the use of a monolayer resist that is not affected by aqueous HF. It has been shown that organic monolayers based on a direct Si–C bond are stable to aqueous HF,³⁴ and the patterning of dodecyl-Si(111) by scanning probe anodization has also been reported.³⁵ Alkyl monolayers may be prepared by thermal, chemical, and photochemical activation of the Si surface in the presence of 1-alkenes.²⁹ We used thermal activation to prepare dodecyl-terminated Si(100) surfaces. On these surfaces, static water contact angles of $108 \pm 1^\circ$ were observed, indicating very good monolayer quality.

Contact mode imaging using a metal-coated cantilever can lead to rapid tip deterioration and corresponding increase in achievable feature size. Accordingly, tapping mode imaging was used while lithography was carried out in contact mode. As tapping mode requires relatively stiff cantilevers, it leads to limited control over the applied force during lithography. It was found that applied forces between 10 and 30 nN yielded reproducible anodization. Oxidized areas were formed by applying a short voltage pulse between the tip and the Si surface. The size of the oxidized area depended on the tip radius as well as the pulse height and duration, and the ambient humidity.³¹

The result of the patterned grafting process is shown in Figure 3. An array of 16 spots was produced by applying a pulse of 9 V for 500 ms under ambient conditions. This initially produced raised oxide features that were then removed by 2% aqueous HF. After dipping in a PbSe nanocrystal solution and rinsing with hexane, the nanocrystals were found to adhere almost exclusively to the areas exposed by the voltage pulse. Around 10–20 nanocrystals were seen in each individual spot, and the density of nanocrystals in the unpatterned areas was again 10 nanocrystals/ μm^2 . Some larger clusters were observed as well; these appeared despite filtering the nanocrystal solution through a 0.02 μm filter, which suggests that they may form on the surface during the deposition process.

Application to Si-based Photonic Crystal Microcavities. The PbSe nanocrystal grafting process was applied to photonic crystal microcavities fabricated on an SOI substrate. The photonic crystal consisted of a hexagonal lattice of holes etched into the intrinsic Si(100) device layer. Using a lattice pitch of 420 nm and a hole radius of 122 nm, L3 microcavities were formed by omitting three etched holes in a row, as seen in Figure 1. The optical modes of the microcavities were characterized by observing the luminescence from a uniform layer of nanocrystals spin-coated on the as-fabricated samples. The resulting spectrum from one L3 cavity with the broadband background luminescence subtracted is shown in Figure 4. The fundamental high-Q mode appears along with higher order cavity modes.³⁶

After fabrication of the microcavity, a dodecyl monolayer was deposited on the sample, and then AFM lithography was carried out as described for normal Si surfaces. The four etched holes closest to the center of the cavity were used as references for positioning the probe tip near the center of the microcavity. Figure 5 shows one sample after nanocrystal

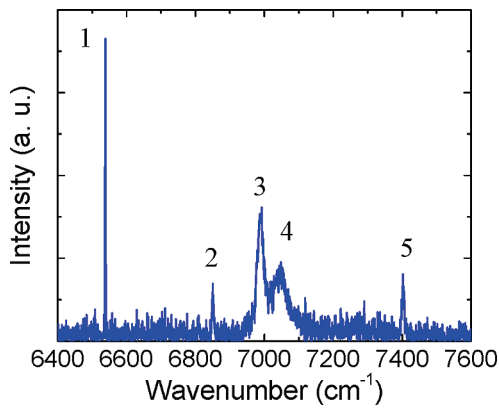


Figure 4. The mode profile of one L3 cavity. The mode 1 is the fundamental mode, and its spatial electric field profile is shown in Figure 1A. The modes 2–5 are other localized modes with lower quality factors.

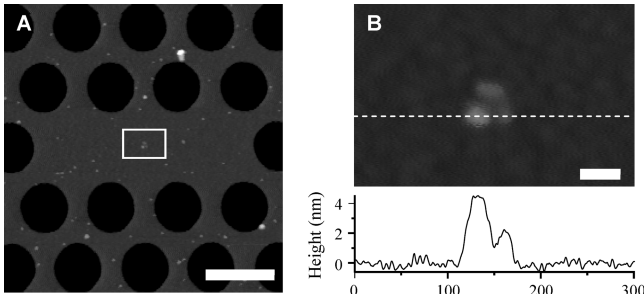


Figure 5. (A) Atomic force micrograph of PbSe nanocrystals grafted to center of Si-based microcavity, and (B) detail of center area with a section along the dashed line. Scale bars are 500 and 50 nm long, respectively.

deposition with a small cluster of nanocrystals located at the center of the microcavity. The lateral dimensions of the nanocrystals are enlarged by the probe tip radius. Although more nonspecific adhesion of PbSe nanocrystals was observed on microcavities than on nonpatterned areas, nanocrystals were always observed to adhere to the desired area at the center of the microcavity. The reduced selectivity most likely arises from an alteration of the interaction with the dodecyl monolayer due to imperfections in the packing imposed by the etched hole boundaries or other etch damage. Along with the presence of randomly adsorbed nanocrystals, this technique positions a small number of nanocrystals with the precision required for coupling to microcavity modes.

The patterning technique reported here thus offers better resolution than the previous report on PbSe nanocrystals patterning using optical lithography^{23,37} and offers much more straightforward registry with submicrometer-scale photonic devices patterned on Si, such as photonic crystal microcavities. Furthermore, possible nanocrystal damage due to intense UV and electron beam radiation is eliminated, and the duration of air exposure can be kept to a minimum. This technique also yielded higher dot density and selectivity with PbSe than with CdSe/ZnS.²⁵

Photoluminescence from Submonolayer Coverages of PbSe. Our PbSe nanocrystals exhibit photoluminescence quantum efficiency up to 40% in solution for emission at $1.55\text{ }\mu\text{m}$, while the efficiency reduces to a few percent in

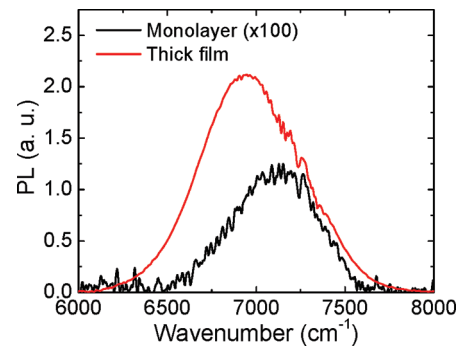


Figure 6. The photoluminescence spectra measured from a sub-monolayer of PbSe (black) and thick drop cast film (red) of the same PbSe solution, both at room temperature. Both spectra were obtained using $1.4 \times 10^2\text{ W/cm}^2$ of HeNe excitation. The curve for the submonolayer sample is multiplied by 100.

drop-cast solid form.³⁸ We found that monolayer coverages of PbSe nanocrystals grafted on H-terminated Si are emissive for several months when kept in vacuum. The sample was excited with a $\sim 2\text{ mW}$ HeNe laser in a micro-PL configuration and the photoluminescence was detected with a Bruker RFS-100 Fourier-transform spectrometer equipped with a Ge detector cooled down to 77 K. Figure 6 shows the room temperature photoluminescence spectrum of a monolayer sample, which was fabricated on a uniform H-terminated SOI wafer by slowly extracting it from the PbSe nanocrystal solution. A spectrum from a several micrometer thick, drop-cast solid layer of the same PbSe solution is also shown for comparison, as thick-film photoluminescence is convenient for rapid determination of emission wavelength. The photoluminescence intensity from the monolayer is much less (~ 200 times) than that from the drop-cast solid layer, but it is strong enough to be detected with the Ge detector. Emission from the thicker film appeared red shifted due to the self-absorption of the higher energy photons (that may be followed by re-emission) and possibly Förster-type migration within the film to larger nanocrystals.

Photoluminescence from Silicon Microcavities with Site-Selectively Attached PbSe Nanoparticles. To demonstrate PbSe coupling to the fundamental L3 microcavity mode, a 5×4 dot array ($400 \times 300\text{ nm}^2$ in total area) was written using AFM lithography at the center of Si-based microcavity that was precoated with a dodecyl monolayer, followed by a HF-dip. The sample was then immediately dipped in the PbSe nanocrystal solution and pulled out slowly. A typical AFM image of these cavities is shown in Figure 7A. The density of PbSe nanocrystals attached to the lithographically defined central region is clearly larger than on the surrounding regions of the microcavity again, exhibiting high grafting preference. The room temperature photoluminescence spectrum from this cavity is shown in Figure 7B, excited with a HeNe laser attenuated to 21 W/cm^2 . A sharp cavity-coupled emission is superimposed on the broad background emission from the noncavity-coupled nanocrystals; a Lorentzian fit to the cavity mode yielded a width of 2.2 cm^{-1} and a Q of 3.1×10^3 . We define the mode contrast as the height of the cavity-coupled emission signal above the noncoupled background signal, normalized to the back-

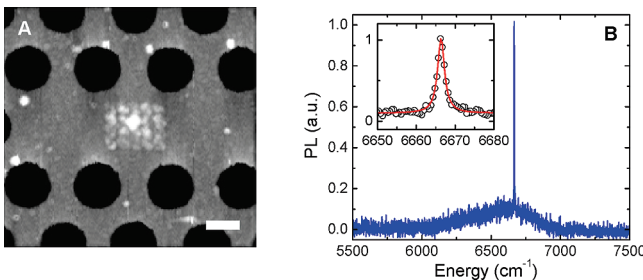


Figure 7. (A) Atomic force micrograph of PbSe nanocrystals grafted to the center of a Si-based microcavity (scale bar 200 nm), and (B) photoluminescence spectrum of the same cavity at room temperature. The inset shows a Lorentzian fit to the cavity mode.

ground at the cavity mode frequency. For the data presented in Figure 7B, the contrast is ~ 9 , which exceeds by more than an order of magnitude the contrast obtained using other techniques^{16,18–20} for coupling nanocrystals to photonic crystal microcavities.

It should be noted that the patterning process does alter the microcavity itself in a small but predictable way. Before the introduction of the emissive nanocrystals, the mode energies of the bare Si cavity can be evaluated using resonant scattering.³⁹ The dodecyl monolayer formation results in a net blueshift of $\sim 80 \text{ cm}^{-1}$ of the microcavity mode. This process step required stripping of the native Si oxide, which removed enough material to shift the microcavity mode to higher energies.^{40,41} The addition of the dodecyl monolayer did not completely compensate for this material removal. The local oxidation and etch steps further remove material in the vicinity of the photonic mode, and this further blue shifts the microcavity modes, as has been reported previously.⁴² After nanocrystal patterning, we have observed an overall blueshift of $\sim 87 \text{ cm}^{-1}$ for the fundamental mode. The cavity Q itself is slightly lowered from 4.0×10^3 to 3.1×10^3 . Nevertheless the cavity Q is also substantially enhanced over previous reports, which is partially due to the cavity design but also to the minimal amount of excess material introduced by the patterning process.

We note that if the randomly adsorbed nanocrystals happen to overlap spatially with the mode antinodes shown in Figure 1B, cavity-enhanced photoluminescence spectra like Figure 7B could also be observed. This was addressed by comparing many side-by-side devices fabricated simultaneously with the patterning process applied to only half of the cavities. The cavity emission contrast can be quantified as the ratio of the cavity mode peak height to the broad background peak emission at the mode frequency, as shown in Figure 8. The patterning process yielded a clear improvement for all 20 pairs of devices considered; cavity emission was observed on all patterned samples, and the contrast was improved in all cases. The average effect of the patterning was a 3-fold increase of photoluminescence contrast. Overall, these results show much better contrast and higher Q factors than previous reports of colloidal nanocrystals coupled to Si-based microcavities.^{16–20}

The contrast improvement could be further increased and made more consistent by reducing nonspecific adsorption of

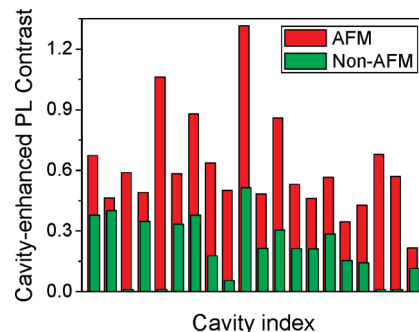


Figure 8. The high- Q mode emission contrast from 20 AFM (red) and non-AFM treated (green) cavities.

the nanocrystals. From the image in Figure 7, it is clear that without rinsing, the number of randomly located nanocrystals on the dodecyl layer away from the patterned region is still significant. Attempts at rinsing away these excess nanocrystals have invariably lead to suppression of the luminescence signal.

Several experiments confirmed that these randomly attached nanocrystals are on both the top and undercut surfaces of the silicon membrane. They therefore have the potential to interact with the cavity mode at all 14 of the strong antinodes on both sides of the silicon membrane shown in Figure 1B, whereas the site-selectively attached nanocrystals can only couple through the center antinode on the top surface. The net impact of the site-selectively located nanocrystals on the overall cavity emission is therefore substantially greater than what might be inferred from the differences between anodized and nonanodized cavity pairs shown in Figure 8.

In conclusion, a method for selectively locating optically active oleate-capped PbSe nanocrystals at the antinode of L3-type photonic crystal microcavities fabricated in silicon-on-insulator-based silicon membranes has been developed. The fabrication process involves using a conducting AFM tip to anodize locally the silicon microcavity at the position of the antinode of the cavity modes, with the rest of the sample protected by a dodecyl monolayer. After dipping in aqueous HF, and then in a solution of PbSe nanocrystals, the nanocrystals are found to attach preferentially to the H-terminated region exposed under the AFM-anodized spot following HF etching. Room temperature photoluminescence reveals the best reported cavity-enhancement of selectively attached PbSe nanocrystal emission from photonic crystal microcavities in Si. This site-selective attachment technique is general and may be easily applied to other nanocrystals capped with the same ligands. With additional refinement, this technique should be capable of controllably localizing few and even single nanocrystal at the cavity antinode maximum.

Acknowledgment. Funding was provided by the Natural Sciences and Engineering Research Council, the Canadian Foundation for Innovation, the British Columbia Knowledge Development Fund, and the Canadian Institute for Advanced Research. We thank J. Madden for use of the atomic force microscope, A. Liu for valuable contributions to the dodecyl monolayer preparation, and J. Buriak for useful comments.

Supporting Information Available: Experimental details including procedures for alkyl monolayer preparation, nanocrystal grafting, and further micrographs and spectra. This material is available free of charge via the Internet at <http://pubs.acs.org>.

References

- (1) Teo, B. K.; Sun, X. H. *J. Cluster Sci.* **2006**, *17* (4), 529–540.
- (2) Woodson, M.; Liu, J. *Phys. Chem. Chem. Phys.* **2007**, *9* (2), 207–225.
- (3) Zhang, X.; Sun, C.; Fang, N. *J. Nanopart. Res.* **2004**, *6* (1), 125–130.
- (4) Khitrova, G.; Gibbs, H. M.; Kira, M.; Koch, S. W.; Scherer, A. *Nat. Phys.* **2006**, *2* (2), 81–90.
- (5) Mabuchi, H.; Doherty, A. C. *Science* **2002**, *298* (5597), 1372–1377.
- (6) Vahala, K. J. *Nature* **2003**, *424* (6950), 839–846.
- (7) Fernee, M. J.; Rubinsztein-Dunlop, H. *Phys. Rev. B* **2006**, *74* (11), 115321.
- (8) Song, B. S.; Noda, S.; Asano, T.; Akahane, Y. *Nat. Mater.* **2005**, *4* (3), 207–210.
- (9) Brunner, K. *Rep. Prog. Phys.* **2002**, *65* (1), 27–72.
- (10) Murray, C. B.; Kagan, C. R.; Bawendi, M. G. *Annu. Rev. Mater. Sci.* **2000**, *30*, 545–610.
- (11) Trindade, T.; O'Brien, P.; Pickett, N. L. *Chem. Mater.* **2001**, *13*, 3843–3858.
- (12) Abel, K. A.; Shan, J.; Boyer, J.-C.; Harris, F. J.; van Veggel, F. C. J. M. *Chem. Mater.* **2008**, *20*, 3794–3796.
- (13) Sargent, E. H. *Adv. Mater.* **2005**, *17* (5), 515–522.
- (14) Stouwdam, J. W.; Shan, J.; van Veggel, F. C. J. M.; Pattantyus-Abraham, A. G.; Young, J. F.; Raudsepp, M. *J. Phys. Chem. C* **2007**, *111* (3), 1086–1092.
- (15) Bose, R.; Yang, X.; Chatterjee, R.; Gao, J.; Wong, C. W. *Appl. Phys. Lett.* **2007**, *90* (11), 111117.
- (16) Dorfner, D. F.; Hürlimann, T.; Abstreiter, G.; Finley, J. J. *Appl. Phys. Lett.* **2007**, *91*, 233111.
- (17) Fushman, I.; Englund, D.; Vuckovic, J. *Appl. Phys. Lett.* **2005**, *87* (24), 241102.
- (18) Vignolini, S.; Riboli, F.; Intonti, F.; Belotti, M.; Gurioli, M.; Chen, Y.; Collocci, M.; Andreani, L. C.; Wiersma, D. S. *Phys. Rev. E* **2008**, *78*, 045603.
- (19) Wu, Z.; Mi, Z.; Bhattacharya, P.; Zhu, T.; Xu, J. *Appl. Phys. Lett.* **2007**, *90* (17), 171105.
- (20) Yang, J.; Heo, J.; Zhu, T.; Xu, J.; Topolancik, J.; Vollmer, F.; Ilic, R.; Bhattacharya, P. *Appl. Phys. Lett.* **2008**, *92*, 261110.
- (21) Akahane, Y.; Asano, T.; Song, B. S.; Noda, S. *Nature* **2003**, *425* (3), 944–947.
- (22) Wang, C. J.; Huang, L.; Parviz, B. A.; Lin, L. Y. *Nano Lett.* **2006**, *6* (11), 2549–2553.
- (23) Lambert, K.; Moreels, I.; Van Thourhout, D.; Hens, Z. *Langmuir* **2008**, *24* (11), 5961–5966.
- (24) Garcia, R.; Martinez, R. V.; Martinez, J. *Chem. Soc. Rev.* **2006**, *35* (1), 29–38.
- (25) Graaf, H.; Vieluf, M.; von Borczyskowski, C. *Nanotechnology* **2007**, *18* (26), 265306.
- (26) Krämer, S.; Fuierer, R. R.; Gorman, C. B. *Chem. Rev.* **2003**, *103*, 4367–4418.
- (27) Tseng, A. A.; Notargiacomo, A.; Chen, T. P. *J. Vac. Sci. Technol., B* **2005**, *23* (3), 877–894.
- (28) Salapaka, S.; Sebastian, A.; Cleveland, J. P.; Salapaka, M. V. *Rev. Sci. Instrum.* **2002**, *73* (9), 3232.
- (29) Buriak, J. M. *Chem. Rev.* **2002**, *102* (5), 1271–1308.
- (30) Li, Q.; Zheng, J.; Liu, Z. *Langmuir* **2003**, *19* (1), 166–171.
- (31) Ling, X.; Zhu, X.; Zhang, J.; Zhu, T.; Liu, M. H.; Tong, L. M.; Liu, Z. F. *J. Phys. Chem. B* **2005**, *109* (7), 2657–2665.
- (32) Yamanoi, Y.; Yonezawa, T.; Shirahata, H. *Langmuir* **2004**, *20* (4), 1054–1056.
- (33) Cho, K.-S.; Talapin, D. V.; Gaschler, W.; Murray, C. B. *J. Am. Chem. Soc.* **2005**, *127* (19), 7140–7147.
- (34) Linford, M. R.; Fenter, P.; Eisenberger, P. M.; Chidsey, C. E. D. *J. Am. Chem. Soc.* **1995**, *117* (11), 3145–3155.
- (35) Ara, M.; Graaf, H.; Tada, H. *Appl. Phys. Lett.* **2002**, *80* (14), 2565–2567.
- (36) Frédéric, S.; Dalacu, D.; Poole, P. J.; Lapointe, J.; Aers, G. C.; Williams, R. L. *Phys. Status Solidi C* **2006**, *3* (11), 3685–3688.
- (37) Kim, W. J.; Kim, S. J.; Lee, K.-S.; Samoc, M.; Cartwright, A. N.; Prasad, P. N. *Nano Lett.* **2008**, *8* (10), 3262–3265.
- (38) Lee, M. H.; Chung, W. J.; Park, S. K.; Kim, M. S.; Seo, H. S.; Ju, J. J. *Nanotechnology* **2005**, *16* (8), 1148–1152.
- (39) McCutcheon, M. W.; Rieger, G. W.; Cheung, I. W.; Young, J. F.; Dalacu, D.; Frederick, S.; Poole, P. J.; Aers, G. C.; Williams, R. L. *Appl. Phys. Lett.* **2005**, *87* (22), 221110.
- (40) Hennessy, K.; Badolato, A.; Tamboli, A.; Petroff, P. M.; Hu, E.; Atature, M.; Dreiser, J.; Imamoglu, A. *Appl. Phys. Lett.* **2005**, *87* (2), 21108.
- (41) Strauf, S.; Rakher, M. T.; Carmeli, I.; Hennessy, K.; Meier, C.; Badolato, A.; DeDood, M. J. A.; Petroff, P. M.; Hu, E. L.; Gwinn, E. G.; Bouwmeester, D. *Appl. Phys. Lett.* **2006**, *88* (4), 043116.
- (42) Hennessy, K.; Hogerle, C.; Hu, E.; Badolato, A.; Imamoglu, A. *Appl. Phys. Lett.* **2006**, *89* (4), 41118.

NL900961R